

# Challenges in Estimating Time-Varying Epidemic Severity Rates from Aggregate Data

Jeremy Goldwasser\*   Addison J. Hu<sup>†</sup>   Alyssa Bilinski<sup>‡</sup>   Daniel J. McDonald<sup>§</sup>  
Ryan J. Tibshirani\*

## Abstract

Severity rates like the case-fatality rate and infection-fatality rate are key metrics in public health. To guide decision-making in response to changes like new variants or vaccines, it is imperative to understand how these rates shift in real time. In practice, time-varying severity rates are typically estimated using a ratio of aggregate counts. We demonstrate that these estimators are capable of exhibiting large statistical biases, with concerning implications for public health practice, as they may fail to detect heightened risks or falsely signal nonexistent surges. We supplement our mathematical analyses with experimental results on real and simulated COVID-19 data. Finally, we briefly discuss strategies to mitigate this bias, drawing connections with effective reproduction number ( $R_t$ ) estimation.

## 1 Introduction

Several public health metrics of interest express the probability that a second, often more serious outcome will follow a primary event. For example, the case-fatality rate (CFR) and infection-fatality rate (IFR) are commonly used to assess the deadliness of an epidemic (Garske et al., 2009; Russell et al., 2020b; Challen et al., 2021; COVID-19 Forecasting Team, 2022; Luo et al., 2021). Another central example of a “severity rate”, which is a term that we use for metrics of this general form, is the hospitalization-fatality rate (HFR) (Bellan et al., 2020; Roth et al., 2021; Xie et al., 2024).

In an ideal setting, severity rates can be obtained directly from a comprehensive line-list or claims data set containing individual patient outcomes (Bellan et al., 2020; Roth et al., 2021; Xie et al., 2024; Challen et al., 2021). However, in fast-moving epidemics like COVID-19, large-scale tracking of individuals has been infeasible, especially in real-time. Instead, severity rates are routinely estimated from aggregate count data. While it is common to assume they are constant in time (Ghani et al., 2005; Jewell et al., 2007; Reich et al., 2012; Baud et al., 2020), consequential shifts in severity rates can occur in response to factors such as new therapeutics, vaccines, and variants (McNeil, 2020). Time-varying severity rates are often estimated with a ratio of primary and secondary aggregate data streams. For example, aggregated case and death data was widely used to report COVID-19 CFRs, both in academic literature (Wjst and Wendtner, 2023; Horita and Fukumoto, 2022; Luo et al., 2021; Yuan et al., 2020; Liu et al., 2023) and major news outlets like The Atlantic (Madrigal and Moser, 2020) and Wall Street Journal (Kamp and Krouse, 2020). In fact, ratio estimators are so common that CFR and IFR are often referred to as case-fatality and infection-fatality *ratios*.

In this work, we show that these ratio estimators are prone to nontrivial statistical bias. Bias arises as a consequence of changing severity rates—precisely when time-varying estimates should be most useful. It also arises due to misspecification of the delay distribution, which relates events, like cases and deaths in CFR. This is particularly troublesome for the popular lagged ratio estimator, which divides values of two aggregate data streams. We validate these findings empirically, tracking the hospitalization-fatality rate (HFR) during COVID-19. The ratio estimators failed to quickly signal increased risk in the onset of the Delta wave; later, in the aftermath of the initial Omicron wave, they surged while the true HFRs fell. We provide heuristics for when to expect this bias in practice, and discuss ideas for alternative methodology which may avoid it.

---

\*Department of Statistics, University of California, Berkeley

<sup>†</sup>Department of Statistics, Carnegie Mellon University

<sup>‡</sup>Brown University School of Public Health

<sup>§</sup>Department of Statistics, University of British Columbia

## 2 Methods

In this section, we introduce the studied estimators, and analyze their bias. Subsequently, we detail the data used for empirical study and validation.

### 2.1 Severity rate estimators

Severity rates convey the probability that a primary event will result in a secondary event in the future. In the case of CFR, for example, a primary event is a positive COVID-19 case, and a secondary event is a death with a positive test result. Formally, the time-varying severity rate at time  $t$  is defined as

$$p_t = \mathbb{P}(\text{secondary event will occur} \mid \text{primary event at time } t). \quad (1)$$

Here,  $t$  may represent a discrete interval of time, like a given day or week. It also may be understood in a continuous-time fashion. For ease of analysis, throughout this paper we consider only discrete timesteps  $t$ , though the same general principles hold in the continuous case.

Let  $\{X\}$  and  $\{Y\}$  denote the aggregate time series of new primary and secondary events. At time  $t$ , we assume data for all past  $s \leq t$  is available, but future data is not. Thus, real-time estimates of severity  $p_t$  can only use counts  $X_{s \leq t}$  and  $Y_{s \leq t}$ .

**Lagged estimator.** The canonical estimator for time-varying severity rates is a ratio between primary and secondary events, offset by a lag  $\ell$ . This lagged approach is formally introduced in [Thomas and Marks \(2021\)](#), but has also been used in prior works (e.g., [Wjst and Wendtner, 2023](#); [Horita and Fukumoto, 2022](#); [Luo et al., 2021](#); [Yuan et al., 2020](#); [Liu et al., 2023](#); [Madrigal and Moser, 2020](#); [Kamp and Krouse, 2020](#)). For real-time estimation, the *lagged ratio* only uses data until the present timestep  $t$ :

$$\hat{p}_t^\ell = \frac{Y_t}{X_{t-\ell}}. \quad (2)$$

To stabilize estimates, smoothed counts are often used in practice ([Wjst and Wendtner, 2023](#); [Luo et al., 2021](#); [Liu et al., 2023](#)). For the sake of simplicity of presentation, we generally focus on the versions described above. However, we formalize the smoothed versions in Equations (9) and (10), and analyze them experimentally.

**Convolutional estimator.** Alternative methods utilize the delay distribution that relates the two time series. The delay distribution is defined as

$$\pi_k^{(t)} = \mathbb{P}(\text{secondary event at } t+k \mid \text{primary event at } t, \text{ secondary event occurs}).$$

Throughout this work, we assume the delay distribution  $\pi$  is the same over all time:  $\pi_k^{(t)} = \pi_k$  for all  $k$  and  $t$ .

While the true delay distributions are generally unknown, several tools exist to estimate them from aggregate or line-list data ([Charniga et al., 2024](#)). Similarly, we truncate the delay distribution at  $d$  days, in essence assuming all secondary events occur within this period. Finally, we assume delay distributions are constant over time, and suppress the dependence on  $t$  in the notation.

The expected number of secondary events at any given day can be expressed in terms of historical primary incidence, severity rates, and the delay distribution ([Qu et al., 2022](#); [Nishiura et al., 2009](#)). Defining  $\mathbb{E}_t[\cdot] = \mathbb{E}[\cdot \mid X_{s \leq t}]$ ,

$$\begin{aligned} \mathbb{E}_t[Y_t] &= \sum_{k=0}^d X_{t-k} \mathbb{P}(\text{secondary at } t \mid \text{primary at } t-k) \\ &= \sum_{k=0}^d X_{t-k} \mathbb{P}(\text{secondary after } k \mid \text{secondary occurs, primary at } t-k) \\ &\quad \times \mathbb{P}(\text{secondary occurs} \mid \text{primary at } t-k) \\ &= \sum_{k=0}^d X_{t-k} \pi_k p_{t-k}. \end{aligned} \quad (3)$$

This is a convolution of the delay distribution against the product of primary incidence and the severity rate. If the severity rate is a constant  $p$ , (3) simplifies to  $\mathbb{E}_t[Y_t] = p \sum_{k=0}^d X_{t-k} \pi_k$ . Nishiura et al. (2009) rearranged this expression to estimate this time-stationary rate. Using a plug-in estimate  $\gamma$  of the delay distribution, and smoothing from time  $t_0$  to  $t$ , they defined

$$\hat{p}_t = \frac{\sum_{s=t_0}^t Y_s}{\sum_{s=t_0}^t \sum_{k=0}^d X_{s-k} \gamma_k}. \quad (4)$$

This estimator is widely used in practice (Garske et al., 2009; Russell et al., 2020b,a). Assuming the true rate is indeed stationary and the delay distribution is correctly specified, it is unbiased. Overton et al. (2022) adapted (4) for the time-varying setting, using only the most recent counts:

$$\hat{p}_t^\gamma = \frac{Y_t}{\sum_{k=0}^d X_{t-k} \gamma_k}. \quad (5)$$

We refer to 5 as the *convolutional ratio*. This estimator can be understood as a generalization of (2). It reduces to the lagged ratio when  $\gamma$  is a point-mass distribution where all secondary events occur after  $\ell$  days. Otherwise, it may relate the two time series more accurately by means of a smooth delay distribution, since the true distribution is unlikely to be a point mass.

Gupte et al. (2024) used the time-varying convolutional ratio to analyze changing COVID-19 CFRs in the UK. The authors implemented Equations (4) and (5) in the R package `cfr`, which is available on CRAN. In general, however, the lagged ratio is the more commonly used time-varying estimator.

**Connection with reproduction numbers.** Severity rates bear natural connections with reproduction numbers. Both the true severity rate as defined in (1) and the case reproduction number  $R_t$  are defined as the average number of secondary events produced by a single primary event at  $t$ . In contrast to severity rates, reproduction numbers have infections as the primary and secondary events, where a single infection can generate more than one secondary event. Comparable to the delay distribution  $\pi$  is the generation interval distribution  $g$ , measuring the time between primary and secondary infections.

Severity rates and reproduction numbers are also estimated similarly. Because primary events at  $t$  produce secondary events after  $t$ , their effect is not observed in real time. Therefore, standard real-time estimates for  $R_t$  and severity rates (2, 5) analyze the number of secondary events at  $t$  produced by relevant primary events. For reproduction numbers, this is formally defined as instantaneous  $R_t$ , the average number of secondary infections at time  $t$  produced by a single primary infection in the past.

Indeed, one of the most popular frameworks to estimate  $R_t$  is based on an almost identical expression to the convolutional ratio (Fraser, 2007; Wallinga and Lipsitch, 2007; Cori et al., 2013; Liu et al., 2024). This expression is a point estimate for instantaneous  $R_t$  derived from the renewal equation:

$$\hat{R}_t = \frac{I_t}{\sum_{k=1}^d I_{t-k} g_k}. \quad (6)$$

The main difference between this ratio and (5) is that (6) uses the same aggregate time series, infections, in both the numerator and denominator. In practice,  $R_t$  is typically estimated in a Bayesian setting, with a posterior obtained from this transmission model. By contrast, the popular estimator from Wallinga and Teunis (2004) is analogous to equation (1), but requires data after time  $t$ .

## 2.2 Well-specified analysis

In this section, we explore the bias of the convolutional ratio (5) when the true delay distribution is known.

**Proposition 1.** *Assume the true delay distribution is a known constant  $\pi$  over all time, where all secondary events must occur within  $d$  timesteps. The bias of the convolutional ratio  $\hat{p}_t^\pi$  is*

$$\text{Bias}(\hat{p}_t^\pi) = \mathbb{E}_t[\hat{p}_t^\pi] - p_t = \sum_{k=0}^d \left[ \frac{X_{t-k} \pi_k}{\sum_{j=0}^d X_{t-j} \pi_j} (p_{t-k} - p_t) \right].$$

Appendix A contains the short proof.

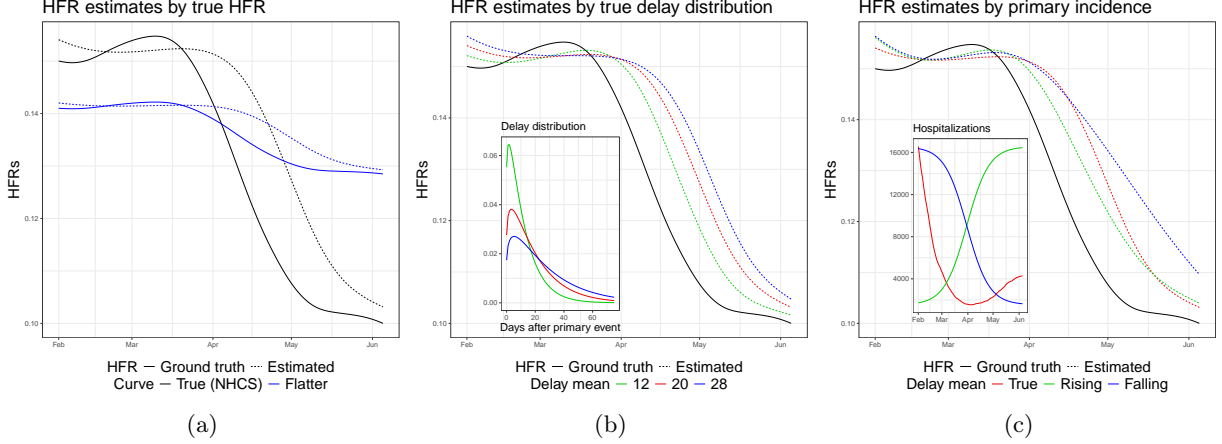


Figure 1: Simple examples of severity rate bias to illustrate the three factors. Deaths were computed noiselessly from (3). Section 2.4 details data sources: NHCS HFRs and real-time HHS hospitalizations in early 2022, and delay distribution estimated with JHU deaths.

The degree of bias in Proposition 1 depends on three factors.

1. **Changes in severity rate.** The central component of this bias expression is the difference  $(p_{t-k} - p_t)$ . When severity rates are constant over the  $d$  preceding days, this estimator is unbiased (because this difference is zero). This is in line with the unbiasedness of the estimator using cumulative counts assuming a globally stationary rate (Nishiura et al., 2009). But when severity rates change before  $t$ , these difference terms will be nonzero, in which case the estimator will be biased.<sup>1</sup> Figures 1a and 13a illustrate this scenario: the estimated severity rates are most inaccurate at periods where the true rate is changing quickly.
- To make matters worse, the bias is in the opposite direction of the trend we want to detect. For example, suppose the severity rate is monotonically falling, with  $p_t < p_{t-1} < \dots < p_{t-d}$ . As a result, the bias is positive, meaning the ratio estimates do not decline with the true rate. In fact, the estimated severity may even rise, not fall. Conversely, when true severity rates are rising, the ratio estimates will be too low.
2. **The delay distribution.** How much the changing severity rates impact the bias depends on the shape of the delay distribution  $\pi$ . In general, the bias is greatest when the delay distribution is long-tailed enough to upweight significant differences in severity rate. While this distinction may appear subtle, Section 3 highlights its surprisingly large effects. The simple example in Figures 1b and 13a shows significant differences in bias between shorter and longer delay distributions.
3. **The primary incidence curve.** Changing primary incidence will also affect the bias, presuming the severity rate changes roughly monotonically in the recent past. Intuitively, this up- or down-weights the terms  $(p_{t-k} - p_t)X_{t-k}\pi_k$  for dates further from the present, which are likely to contribute the most bias. In general, falling primary incidences will amplify the bias, whereas rising events will minimize it; see Appendix D.2 for more detail. Figures 1c and 13b visualize this trend on the convolutional ratio.

Appendix D.2 discusses toy settings in which the well-specified bias simplifies in elucidating ways.

## 2.3 Misspecified analysis

The above section considered the bias of the convolutional ratio where the true delay distribution  $\pi$  is known. We now consider the more general case, in which it is instead replaced with a plug-in estimate  $\gamma$ . Note the bias of the lagged estimator is a special case, where the plug-in distribution is a point mass at lag time  $\ell$ .

<sup>1</sup>It is possible that this estimator could still be unbiased in the unlikely event that individual components in the summation over  $k$  exactly cancel each other.

**Proposition 2.** Assume that the true delay distribution  $\pi$  is constant over time and that its maximal length  $d$  exceeds that of the plug-in distribution  $\gamma$ . Define  $A_t^\gamma = \sum_{j=0}^d X_{t-j}\pi_j / \sum_{j=0}^d X_{t-j}\gamma_j$ , which compares how the delay distributions convolve against the most recent primary incidence levels. The misspecified bias is

$$\text{Bias}(\hat{p}_t^\gamma) = A_t^\gamma \text{Bias}(\hat{p}_t^\pi) + p_t(A_t^\gamma - 1).$$

For the lagged estimator, (2) becomes

$$\text{Bias}(\hat{p}_t^\ell) = \frac{\sum_{j=0}^d X_{t-j}\pi_j}{X_{t-\ell}} \text{Bias}(\hat{p}_t^\pi) + p_t \left( \frac{\sum_{k=0}^d X_{t-k}\pi_k}{X_{t-\ell}} - 1 \right). \quad (7)$$

Proposition 2, proven in Appendix A, provides an additive decomposition of the misspecified ratio's bias. The first term scales the oracle bias, whereas the other solely expresses misspecification. In both terms,  $A_t^\gamma$  dictates the extent to which the misspecified distribution alters the bias. This term expresses how the delay distributions convolve against the primary incidence curve. When  $A_t^\gamma = 1$ , the bias reduces to the oracle case. Values of  $A_t^\gamma > 1$  will amplify the oracle bias and add positive misspecification bias. Otherwise,  $A_t^\gamma < 1$  shrinks the oracle bias and adds negative misspecification bias.

Curves with  $A_t^\gamma > 1$  tend to have more positive bias than the oracle ratio, while  $A_t^\gamma < 1$  contributes negative bias (Figure 2, 4). The rescaled oracle and misspecification terms move together when oracle bias is positive. In theory, they are at odds with one another when oracle bias is negative. For example,  $A_t^\gamma > 1$  draws oracle bias further below 0, while adding positive misspecification error. However, the misspecification term consistently wins out when this occurs in our experiments. Section 3.2 discusses this and other empirical findings in greater depth.

We detail the behavior of  $A_t^\gamma$  in common settings of interest, under three standard delay distributions.

1. Smooth delay distribution with a lighter tail than the true distribution  $\pi$ , and more mass concentrated at recent dates.
2. Smooth delay distribution with a heavier tail and lower mean than  $\pi$ .
3. Lagged delay distribution, a point mass at  $\ell$ . We refer to its ratio  $A_t^\gamma$  as  $A_t^\ell$ . Let  $\ell$  be near the mean of  $\pi$ .

**Primary incidence rising.** Consider the case where primary events are rising — first slowly, then rapidly before leveling off. A light-tailed  $\gamma$  will place more weight on recent dates with high counts than  $\pi$ . Then  $\sum_{j=0}^d X_{t-j}\gamma_j > \sum_{j=0}^d X_{t-j}\pi_j$ , so  $A_t^\gamma < 1$ . The opposite occurs for heavy-tailed  $\gamma$ . Relative to  $\pi$ ,  $\gamma$  convolves with more weight on the distant low-count dates, and less on the ongoing surge. This trend holds from the beginning of the wave through its peak.

The plug-in distribution  $\gamma_k = \mathbb{1}\{k = \ell\}$  convolves all its mass at  $X_{t-\ell}$ . During the steepest phase of the rise, this is considerably lower than  $X_t$ . In contrast,  $\pi$  distributes mass across the  $d$  trailing dates. Roughly half of its mass convolves the last  $\ell$  days, whose counts exceed  $X_{t-\ell}$ . The dates before  $t - \ell$  have less of an offsetting effect, since incidence has risen at a growing rate. Therefore  $\sum_{j=0}^d X_{t-j}\gamma_j > X_{t-\ell}$ , so  $A_t^\ell > 1$ .

Figure 2 visualizes this on simulated deaths as hospitalizations rise between December 2021 and mid-January 2022. Throughout the entire rise,  $A_t^\gamma$  is below 1 for the light-tailed distribution, and above 1 with the heavy tail. Meanwhile,  $A_t^\ell$  spikes to 1.2 during the quick rise in the first half of January. This corresponds to the lagged HFR rising to 20%, while the true HFRs fall to 15%.

**Primary incidence begins falling.** Next, assume primary incidence reaches a maximum and begins to fall. The smooth distributions behave much the same as when incidence was rising. The lower-mean distribution has more mass around the peak than  $\pi$ , so  $A_t^\gamma < 1$ . Conversely,  $A_t^\gamma > 1$  for the heavier-tail distribution because it convolves more mass before the top of the rise.

The lagged bias changes its behavior in this period. While  $A_t^\ell$  had exceeded 1 before the peak, it quickly plunges below 1. In fact,  $\ell$  days after the peak, the lagged estimator attains the smallest possible value of  $A_t^\gamma$ , since  $X_{t-\ell}$  maximizes its denominator  $\sum_{j=0}^d X_{t-j}\gamma_j$ .

In general,  $A_t^\gamma$  is most extreme when  $\gamma$  is a point-mass distribution at the maximal or minimal value of  $X_{t-d}, \dots, X_t$ . This inevitably occurs with the lagged estimator as its convolution sweeps across the primary incidence curve. The convolutional ratios do not reach such extremes by nature of their smooth delay distributions. Hence, the lagged ratio is likely to have larger fluctuations of  $A_t^\ell$ , and thus higher bias. In some settings, it may even attain the worst-case delay distribution in Proposition 2.

In Figure 2,  $A_t^\ell$  reaches 0.8 around the beginning of February 2022. This is precisely  $\ell = 16$  days after daily new hospitalizations peak above 20,000 in mid-January. The lagged ratio falls accordingly from 20% to 13%, with the true HFRs remaining roughly constant at 15%. In the same period, the misspecified convolutional ratios stay within 2% of the true HFR.

**Primary incidence levels out from a fall.** The most jarring instance of misspecification bias occurs as primary incidence continues to fall, then levels out. By construction, the true delay distribution has a heavier tail than the low-mean, light-tailed distribution. It also has a heavier tail than the lagged point mass, which has no tail at all. This has important implications as the peak of the surge fades into the past, and primary incidence levels out. Compared to  $\pi$ , the light-tailed and lagged distribution convolve little to no mass with the high-count period of the surge. As a result,  $A_t^\gamma$  and  $A_t^\ell$  both rise above 1. The magnitude of the spike depends on the size of the change in primary incidence.

Figure 2 displays this false spike. Around late March 2022,  $A_t^\gamma$  and  $A_t^\ell$  reach a maximum near 1.2 and 1.5, respectively. Their corresponding HFRs reach 18% and 22% while the true HFR is only 15%.

The opposite trend occurs for the heavier-tailed delay distribution. More of its mass convolves with the top of the surge than  $\pi$ , so its  $A_t^\gamma < 1$ . Figure 2 shows it minimizing at 0.8 in April 2022. Its convolutional ratio has about 2% lower HFR than the oracle curve.

## 2.4 Experimental setup

[JMG: Should it be its own whole section?]

**Hospitalization-fatality rate.** Our experiments analyze the HFR throughout COVID-19. While HFR is less commonly reported than CFR, it has a few advantages as an object of study. Firstly, time-varying HFR estimates for the US can be validated with a line list. The "Validation data" section below describes this in detail. To our knowledge, no such resource exists for CFR.

In addition, hospitalization reporting was much more complete than case reporting throughout the pandemic. Hospitals were mandated to report new daily admissions to the Department of Health and Human Services (HHS) or face penalties ([Department of Health and Human Services, 2023](#)).

Lastly, our analysis assumes the true time-to-death delay distribution has non-negative support. This holds true for HFR, since COVID hospitalizations are aligned by admission date. For CFR, however, cases may be reported after deaths due to long reporting delays. Cases were sometimes reported up to 45 days after infection ([Jahja et al., 2022](#)); meanwhile, [Zhou et al. \(2020\)](#) studied a cohort in which the median infection-to-death time was only 18 days. Nevertheless, negative case-to-death delays are uncommon enough that the same findings should apply for both CFR and HFR [Russell et al. \(2020b\)](#); [Ward and Johnsen \(2021\)](#).

**Aggregate data.** To estimate real-time HFRs, we use daily hospitalizations and deaths as available in the `epidatr` API, developed by the Delphi Group. Like HHS for hospitalizations ([Department of Health and Human Services, 2023](#)), John Hopkins University (JHU) provided the definitive resource for real-time death counts ([Center for Systems Science and Engineering \(CSSE\) at Johns Hopkins University, 2023](#)). These counts reflect the times at which deaths were reported to health authorities, not necessarily when they actually happened. Therefore raw JHU death counts are highly volatile due to reporting idiosyncrasies like day-of-week effects and data dumps. As a result, we used a 7-day trailing average of counts.

Because the daily aggregates from JHU and HHS were updated over the course of the pandemic, we use both the counts available in real time as well as their finalized versions. Occasionally, the most recent date with available counts lagged several days behind the present. To account for this, we estimated HFRs each

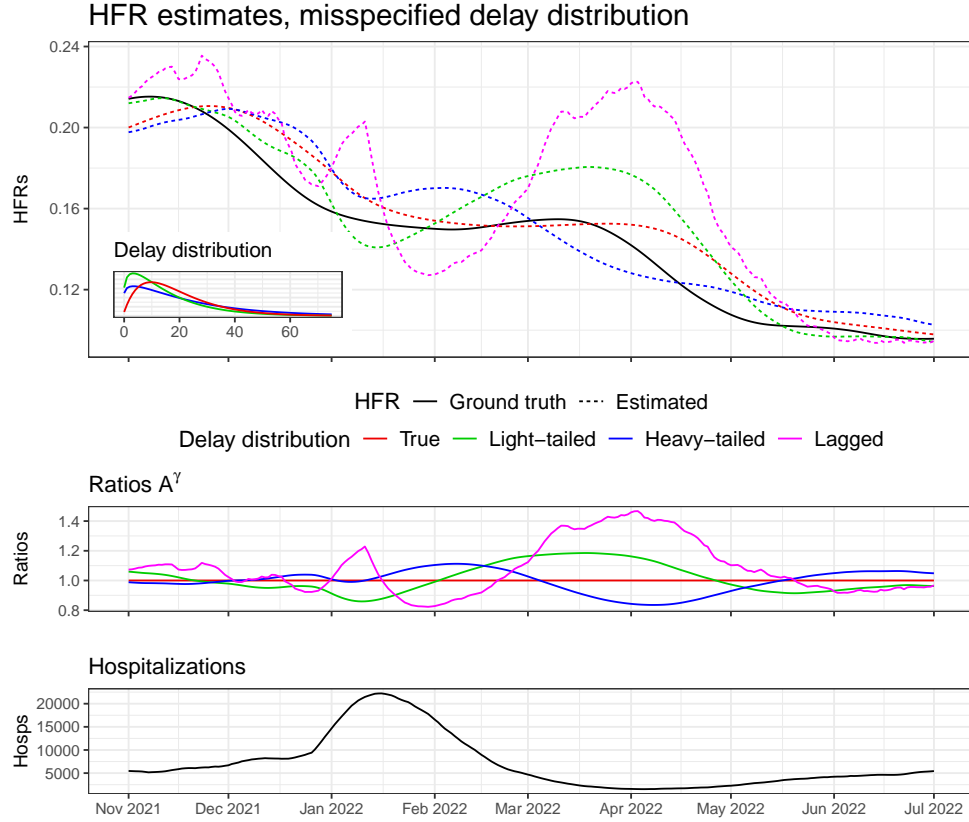


Figure 2: HFR estimates under misspecification. HHS hospitalizations, NHCS HFRs, and noiseless deaths from (3) (Section 2.4). True delay distribution is gamma with mean of 20 days. Convolutional ratio estimates use oracle delay distribution, misshapen gammas (mean 16 and 24), and point mass at correlation-maximizing lag (16).



week, using real-time data that was available two days after each date. Therefore the real-time estimates are actually a two-day backcast of the HFR. In the rare event that requested counts were still unavailable, we imputed the value with the most recently observed data.

**Hyperparameters.** The ratio estimators studied require choices of lag and delay distribution. Appendix C evaluates the robustness of findings against different hyperparameter values. The experiments in Section 3.1 use a lag of 20 days, which maximizes the cross-correlation between hospitalizations and deaths over all time (Madrigal and Moser, 2020).

We let the delay distribution be a discrete gamma, a common choice Charniga et al. (2024). We set its length  $d$  to 75 days, a conservative choice. For its mean, we used the oracle lag above, as lags are often chosen to be the mean of the delay distribution. This mean of 20 matches nicely with a UK study that finds a median hospitalization-to-death time of 11 days (Ward and Johnsen, 2021), and a CDC report that 63% of COVID deaths are reported within 10 days (Centers for Disease Control and Prevention, National Center for Health Statistics, 2023). We set the standard deviation to 18, because the delay distributions fit by the UK study had standard deviations that were roughly 90% of their means.

It is worth noting that conditions in the UK may be quite different from the US. However, we use this paper’s findings because it provided the most comprehensive information on COVID hospitalization-to-death delay distributions.

**Validation data.** While the true HFRs are unknown, there are sound ways to approximate them. One such approach is to use line-list HFRs from the National Hospital Care Survey (National Center for Health Statistics (NHCS), 2023). The NHCS recorded weekly HFRs from inpatient deaths in a representative subset of 601 hospitals across the US.

HFRs from aggregate hospitalization and death counts are significantly higher than those from NHCS because not all deaths occur in hospitals. A CDC analysis reported the percentage of inpatient deaths every month from 2020 through 2022; roughly 60% of COVID deaths occurred in hospitals in 2022, down from nearly 70% in 2021 and 2022. To account for non-inpatient deaths, we divided the NHCS curve by these percentages. Finally, we smoothed the resulting HFRs with a spline. To do so, we used the `smooth.spline` function in R, which chooses the smoothness hyperparameter with generalized cross validation.

The NHCS curve is a useful benchmark to judge the fidelity of our HFR estimates. Of course, its values may be inaccurate because it surveys a relatively small subset of hospitals. Results in Section 3 suggest it is too high in late 2022. Appendix B.2 discusses other approximations of ground truth HFRs.

## 3 Results

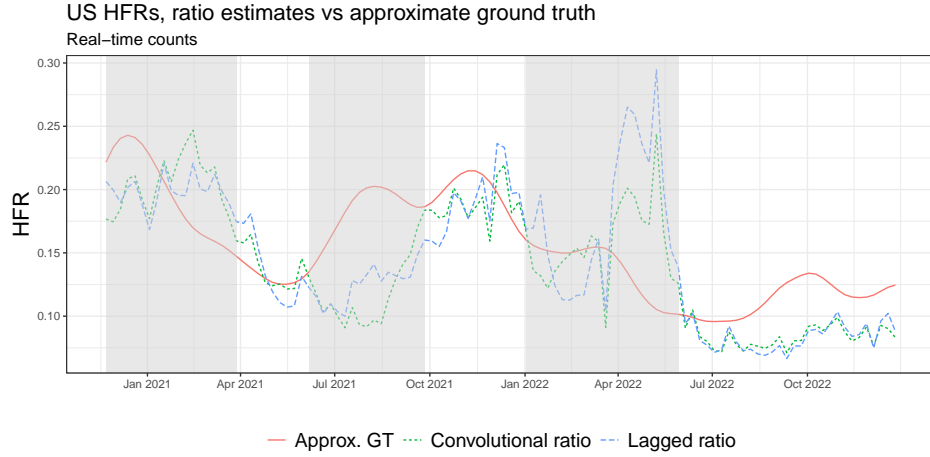
In this section, we explore the performance of the ratio estimators in greater depth. We analyze HFR estimates on real data in Section 3.1, and simulated data in Section 3.2. Throughout both, we continue to use aggregate hospitalization counts from HHS throughout the COVID-19 pandemic.

### 3.1 COVID-19 data

Figure 3 displays real-time HFR estimates on the data described in Section 2.4. We computed HFRs from November 2020 to December 2022, spanning the major COVID variants. The real-time hospitalization and death counts exhibit a fair degree of instability, so we preprocessed them with seven-day smoothing. Even then, the basic HFRs (5) and (2) still had a few days with wild spikes. To smooth these artifacts away, we further applied a seven-day trailing window to the ratio estimators, as in (9) and (10). Figure 8 in Appendix C examines how trailing window length affects HFR estimates.

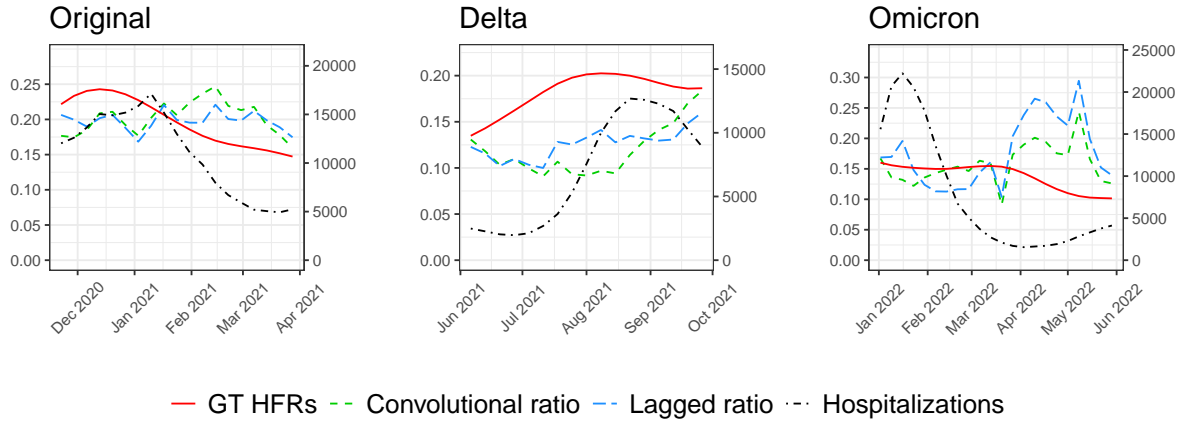
Overall, both ratio estimators perform very poorly. As described in Propositions 1 and 2, the bias is consistent and nontrivial, especially for the lagged estimator. Both the lagged and convolutional ratios respond very slowly to changes in the HFR. As the HFR declines following the wave in winter 2021, both ratios remain near 0.2 for several months. More troublingly, they are very slow to detect the rising HFR in the early Delta period (summer 2021). If the purpose of these estimators is to inform stakeholders of increased risks in real time, they failed during the Delta surge.





(a) Comparing convolutional and lagged ratios against approximate ground truth.

### HFRs and hospitalizations by wave



(b) HFRs and hospitalizations in three periods with major bias.

Figure 3: HFR estimates from real-time aggregates, Nov. 2020 — Dec. 2022. Biased periods of major waves are highlighted.

The most significant bias comes in the middle of the Omicron wave in spring 2022. In this period, the HFR remains around 15% until April, then sharply declines to 9% two months later. The lagged ratios first fluctuate above and below the true HFRs. Subsequently, both estimates surge as the true HFR nears its nadir, with the lagged ratio nearing 30%. This dramatic upswing signals a serious false alarm. The analysis in Sections 2.2 and 2.3 explain each of these failure cases.

**Well-specified analysis.** We start by analyzing the convolutional ratio with respect to the well-specified bias expression in Proposition 1. While this expression assumes that the true delay distribution is known, we found that different choices of delay distribution generally yield similar bias (Appendix C). This indicates that our estimates may not be far from the oracle ratio.

Proposition 1 indicates that the bias moves in the opposite direction of the true severity rate. This occurs during the Delta wave, when the HFRs rise well before the ratio estimates do. Conversely, falling HFRs produce positive bias, as observed in the original and Omicron waves.

The enormity of the bias during Omicron can partially be attributed to the precipitous decline in hospitalizations, as falling primary incidence has been shown to exacerbate the bias. Average daily hospitalizations declined from over 20,000 in mid-January to only 1,500 by April 1. Finally, the delay distribution is relatively long with JHU deaths due to its alignment by report date. This is shown to have a substantial impact on the bias, as analyzed in Appendix B.1.

**Misspecified analysis.** The misspecification analysis explains central discrepancies between the convolutional and lagged ratios. Section 2.3 discusses how  $A_t^\ell < 1$  in the initial weeks of declining primary incidence. As a result, the lagged ratio should incur negative misspecification error. We observe this when hospitalizations with the original variant fall from their peak in mid-January 2021. Throughout February, lagged estimates are about 2% below the positively biased convolutional ratios.

When primary incidence rises,  $A_t^\ell > 1$ , contributing positive bias relative to the oracle convolutional ratio. Correspondingly, as hospitalizations surge due to the Delta variant in August 2021, the lagged ratio is less negatively biased.

Lastly, we explained that  $A_t^\ell > 1$  after a fall in primary incidence. This accounts for the lagged ratio having higher bias in April 2022, when hospitalizations level out from the Omicron surge. Figure 2 visualizes this same period, where the true HFRs and delay distribution are known. There,  $A_t^\ell$  reaches 1.5, by far its maximum — validating the magnitude of the difference between the convolutional and lagged ratios.

We performed several robustness checks to assess the stability of these findings. Appendix C explores the effect of different hyperparameters and locations. By and large, the ratio estimators yield roughly the same bias regardless of these considerations. It also compares HFR estimates using finalized counts, rather than the data available in real time. This exploration finds that the observed biases could not be attributed to real-time reporting issues.

### 3.2 Simulated data

We further evaluated these methods in a variety of simulation settings. Given a series of time-varying HFRs  $p_t$  and delay distribution  $\pi$ , deaths are defined without noise from (3):

$$Y_t = \sum_{k=0}^d X_{t-k} \mathbb{P}(\text{die at } t \mid \text{hosp at } t-k) = \sum_{k=0}^d X_{t-k} \pi_k p_{t-k}.$$

Like the experiments in Sections 2.2 and 2.3, we used real-time HHS hospitalization counts. The simulations in this section evaluate performance over a two-year period, with a broader range of underlying HFR curves. To supplement the NHCS HFRs, we mimicked the opposite trend by inverting and rescaling them. We also modeled a stationary HFR of 10% over all time. As in Section 2.4, the delay distributions were again gamma with standard deviation 0.9 of their mean. We experimented with means of 12 and 24 to illustrate a short and long delay distribution.

To elucidate the oracle bias in Proposition 1, we let the convolutional ratio use the true delay distribution. For the lagged ratio,  $\ell$  was again chosen to maximize the cross-correlation between hospitalizations and

## HFRs, simulated deaths

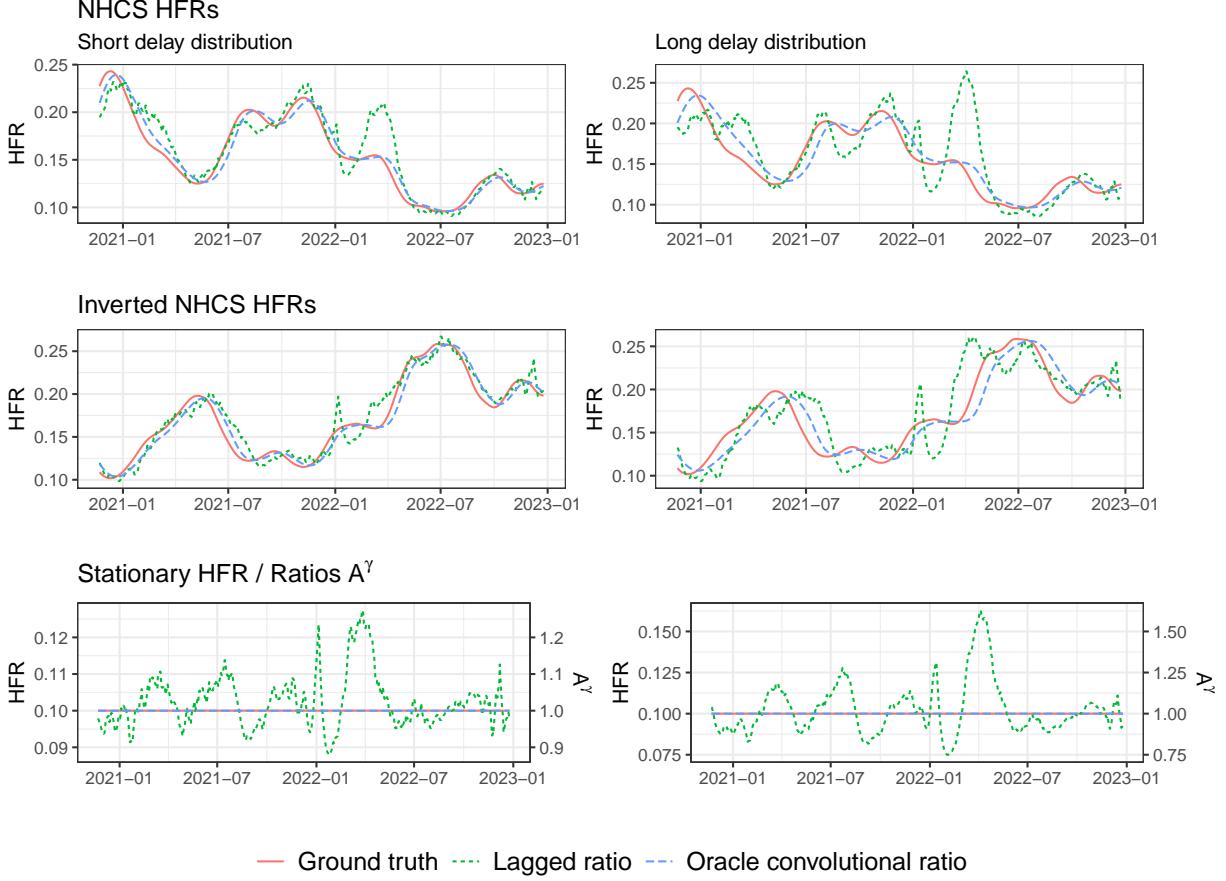


Figure 4: True and Estimated HFRs from Simulated Deaths. First column has short delay distribution, second has long.

deaths. We also experimented with the mean of the delay distribution, as advocated by [Feng et al. \(2023\)](#). Figure 12 in Appendix D shows the results are similarly unstable.

Figure 4 displays the results on the six settings of delay distribution and HFR. Matching expectations, HFRs are significantly more biased given the longer underlying delay distribution. In all three HFR settings, the lagged ratios swing more widely. For example, when the true HFR is a constant 10%, they peak at 12% under the light-tailed distribution, compared to 15% with the heavy tail. The oracle convolutional ratio does not share the lagged estimator’s dramatic oscillations. Rather, it tracks the general shape of true curve, albeit at a delay. For the NHCS HFRs, the average delay was 5 days for the light-tailed distribution, and 12 days with heavy tail; these delays were 6 and 14 days for the inverted curve. (To compute the average delay, we again took the maximal cross-correlation between the two series.)

The analysis in Section 2.3 accounts for the wide gap in performance between the two estimators. Proposition 2 expresses bias under misspecification as a function of the ratio  $A_t^\gamma$ . These ratios  $A_t^\gamma$  are visualized in Figure 4 as rescaled HFR estimates in the stationary case. Given a constant rate  $p$ , the oracle convolutional ratio is unbiased, so Proposition 2 reduces to  $\mathbb{E}[\hat{p}_t^\gamma] = pA_t^\gamma$ . Furthermore,  $\mathbb{E}[\hat{p}_t^\gamma] = \hat{p}_t^\gamma$ , as our setup simulates deaths without noise. Consequently,  $A_t^\gamma = \frac{\hat{p}_t^\gamma}{p}$ .

In expectation, the lagged ratio is higher than the oracle convolutional ratio when  $A_t^\gamma > 1$ , and lower when  $A_t^\gamma < 1$ . Comparing the  $A_t^\gamma$  curves to the estimated HFRs, the bias moves very similarly. For example, during the Delta and Omicron waves, rapid rises in hospitalizations produced high values of  $A_t^\ell$ . This accounts for the spikes in August 2021 and January 2022. When hospitalizations level out from the Omicron surge,  $A_t^\ell$

spikes to 1.2 and 1.5 for the short and long distributions — hence the positive bias in spring 2022. Lastly, the lagged estimator should have negative bias as primary events fall. We observe this in Delta (September 2021) and Omicron (February 2022).

The misspecified bias (Proposition 2) rescales the oracle bias and adds a misspecification term. Studying Figure 4, we observe the misspecification term tends to dominate when  $A_t^\gamma$  strays away from 1. To understand this, consider periods in which the oracle bias is negative. As introduced in Section 2.3, the oracle and misspecification terms are at odds with each other when this is the case.

Invariably, the lagged ratio moves in the direction of the misspecification term  $p_t(A_t^\gamma - 1)$ . Under the true NHCS HFRs, for example, the lagged estimates spike with  $A_t^\ell$  in August 2021. In the inverted setting, the lagged bias tracks the down-up-down motion of  $A_t^\ell$  during the first five months of 2021. That the misspecification term wins out in these conflicting settings indicates it comprises a disproportionate amount of the bias. Indeed, the oracle bias is generally low enough that multiplicative rescaling may not have a large effect.

For a further example, consider the bias at April 2022 on the middle right. The true HFR is 14%, with the convolutional ratio nearby at 15%. Meanwhile, the lagged ratio peaks at 22.5%, driven upwards by an  $A_t^\ell$  of 1.5. Decomposing the lagged bias of 8.5% with Proposition 2, the oracle term  $A_t^\ell \text{Bias}(\hat{p}_t^\pi)$  equals only 1.5%; meanwhile, the misspecification term  $p_t(A_t^\ell - 1) = 7\%$ , accounting for the majority of the bias.

## 4 Discussion

Our analyses illustrate that practitioners should take caution when using time-varying severity ratio estimators. They exhibit considerable bias when severity rates change, particularly the popular lagged ratio estimator. A major purpose of these estimators is to inform stakeholders of changing risks in real time; this bias indicates they may fail to do so in a reliable manner.

Analyzing the lagged ratio enables us to make real-time heuristics about its performance in practice. Proposition 2 decomposes its bias into oracle and misspecification terms, the latter of which has been shown to dominate. Based solely on the primary incidence curve, we can expect the lagged ratio to make the following errors:

1. Unreasonably high severity estimates when primary incidence is rising quickly;
2. Rapid declines when primary incidence is falling quickly;
3. Unexpected surges when primary incidence has leveled out after falling.

Practitioners can adjust their reactions accordingly when these bias patterns occur in real time. For example, if the lagged HFR spikes shortly after hospitalizations reach a stable low, a savvy epidemiologist can temper her alarm with the knowledge it may well be spurious.

While the lagged ratio is ubiquitous in practice, our analysis of its drawbacks suggests other aggregate estimators should be favored. Figure 4 showed the oracle convolutional ratio is much more accurate. It still outperformed the lagged ratio given a misspecified delay distribution, though its bias was also large (Figures 2 and 3).

Qu et al. (2022) proposed an approach that differs considerably from the ratios discussed in this paper. The method estimates all historical severity rates at once, using the relation in (3) to fit a fused lasso model. This estimator is inherently forward-looking, where rates at  $t$  are exclusively used to produce secondary events after  $t$ . Given regularization parameter  $\lambda$ , current time  $T$ , and start time  $t_0$ , the fused lasso estimates

$$\hat{p}^{\text{FL}} = \underset{p \geq 0}{\text{argmin}} \sum_{t=t_0}^T (Y_t - \sum_{j=0}^d X_{t-j} \gamma_j p_{t-j})^2 + \lambda \sum_{t=t_0-d+1}^T |p_t - p_{t-1}|.$$

This estimator is not succumb to the issues of the backward-looking ratios. However, it may suffer from other sources of bias. It is inclined to estimate smoothly-changing severity rates as piecewise constant, and may yield unstable real-time estimates due to scarce data at the tail. Thorough investigation of its performance is a promising object for future study.

Future work could generalize the above approach beyond piecewise constants. The fused lasso is a special case of trend filtering, a nonparametric regression technique that fits piecewise polynomials Tibshirani (2014). Higher-order curves may better model trends and improve performance. (Jahja et al., 2022) applies trend filtering to a similar deconvolution problem, reconstructing latent infections from case reports. Its insights on tail regularization may be useful to stabilize severity estimates.

Overton et al. (2022) also proposed a forward-looking method, this one a ratio between relevant primary and secondary events. However, this method is not applicable in real time, as it uses secondary events after  $t$  to compute the severity rate. Nevertheless, it is a useful tool for retrospective estimation.

Another retrospective tool is aggregate COVID deaths from NCHS, a resource that was not available in real time (Appendix B.1). Unlike JHU, whose aggregates align deaths by report date, NCHS counts deaths on the day the actually occurred. As a result, the mean of its delay distribution is considerably lower, so it produces more accurate ratio estimates (Figures 4 and 5). Analogously, bias is a more serious issue with earlier primary events. For example, case- or infection-fatality ratios may be more biased than hospitalization-fatality ratios.

Severity rates may be biased in ways beyond the statistical bias our work focuses on. In Section 2.4, we mentioned that HFR estimation from aggregates is subject to survivorship bias — the failure to account for deaths that occurred outside the hospital (Lipsitch et al., 2015). Under-reporting is another central challenge, particularly for CFR. Not all infections are reported, reporting rates change across time, and severe cases are more likely to be reported than mild cases. Reich et al. (2012) proposed an estimator for a time-invariant *relative* CFR — the ratio of CFRs between groups — that learns these latent reporting rates via the EM algorithm (Dempster et al., 1977). Angelopoulos et al. (2020) applied this in the context of COVID-19, analyzing how the chosen delay distribution affects its results. The work also identifies other sources of bias, like differences in case definition and testing eligibility.

As discussed in Section 2.1, severity rates may be understood in connection with reproduction numbers. This connection extends to their bias as well. For example, we demonstrated that the convolutional ratio is unbiased if the severity rate and delay distribution in the  $d$  days before  $t$  are stationary. In a similar vein, Fraser (2007) noted that instantaneous  $R_t$  is equal to case  $R_t$  if conditions remain unchanged. Future work along the lines of Eales and Riley (2023) could apply our analytical framework to  $R_t$  bias, examining the fidelity of instantaneous  $R_t$  as a proxy for case  $R_t$ .

## References

- Adjei, Stacey and Hong, Kai and Molinari, Noelle-Angelique M and Bull-Otterson, Lara and Ajani, Umed A and Gundlapalli, Adi V and Harris, Aaron M and Hsu, Joy and Kadri, Sameer S and Starnes, Jon and Yeoman, Kristin and Boehmer, Tegan K (2022). Mortality risk among patients hospitalized primarily for covid-19 during the omicron and delta variant pandemic periods - united states, april 2020-june 2022. *MMWR Morb Mortal Wkly Rep*, 71(37):1182–1189.
- Angelopoulos, A. N., Pathak, R., Varma, R., and Jordan, M. I. (2020). On Identifying and Mitigating Bias in the Estimation of the COVID-19 Case Fatality Rate. *Harvard Data Science Review*, (Special Issue 1). <https://hdsr.mitpress.mit.edu/pub/y9vc2u36>.
- Baud, D., Qi, X., Nielsen-Saines, K., Musso, D., Pomar, L., and Favre, G. (2020). Real estimates of mortality following COVID-19 infection. *Lancet Infectious Diseases*, 20(7):773. Epub 2020 Mar 12.
- Bellan, M., Patti, G., Hayden, E., Azzolina, D., Pirisi, M., et al. (2020). Fatality rate and predictors of mortality in an Italian cohort of hospitalized COVID-19 patients. *Scientific Reports*, 10:20731.
- Center for Systems Science and Engineering (CSSE) at Johns Hopkins University (2023). Covid-19 data repository. GitHub repository.
- Centers for Disease Control and Prevention, National Center for Health Statistics (2023). Deaths by select demographic and geographic characteristics. Archived September 27, 2023.

- Challen, R., Brooks-Pollock, E., Read, J. M., Dyson, L., Tsaneva-Atanasova, K., and Danon, L. (2021). Risk of mortality in patients infected with SARS-CoV-2 variant of concern 202012/1: Matched cohort study. *British Medical Journal*, 372:n579.
- Charniga, K., Park, S. W., Akhmetzhanov, A. R., Cori, A., Dushoff, J., Funk, S., Gostic, K. M., Linton, N. M., Lison, A., Overton, C. E., Pulliam, J. R. C., Ward, T., Cauchemez, S., and Abbott, S. (2024). Best practices for estimating and reporting epidemiological delay distributions of infectious diseases using public health surveillance and healthcare data.
- Cori, A., Ferguson, N. M., Fraser, C., and Cauchemez, S. (2013). A new framework and software to estimate time-varying reproduction numbers during epidemics. *American Journal of Epidemiology*, 178(9):1505–1512.
- COVID-19 Forecasting Team (2022). Variation in the COVID-19 infection–fatality ratio by age, time, and geography during the pre-vaccine era: A systematic analysis. *Lancet*, 399(10334):1469–1488.
- Dempster, A. P., Laird, N. M., and Rubin, D. B. (1977). Maximum likelihood from incomplete data via the em algorithm. *Journal of the Royal Statistical Society. Series B (Methodological)*, 39(1):1–38.
- Department of Health and Human Services (2023). Covid-19 guidance for hospital reporting and faqs for hospitals, hospital laboratory, and acute care facility data reporting.
- Eales, O. and Riley, S. (2023). Differences between the true reproduction number and the apparent reproduction number of an epidemic time series.
- Feng, J., Luo, H., Wu, Y., Zhou, Q., and Qi, R. (2023). A new method for accurate calculation of case fatality rates during a pandemic: Mathematical deduction based on population-level big data. *Infectious Medicine*, 2(2):96–104.
- Fraser, C. (2007). Estimating Individual and Household Reproduction Numbers in an Emerging Epidemic. *PLOS ONE*, 2(8):1–12.
- Garske, T., Legrand, J., Donnelly, C. A., Ward, H., Cauchemez, S., Fraser, C., Ferguson, N. M., and Ghani, A. C. (2009). Assessing the severity of the novel influenza A/H1N1 pandemic. *British Medical Journal*, 339:b2840.
- Ghani, A. C., Donnelly, C. A., Cox, D. R., Griffin, J. T., Fraser, C., Lam, T. H., Ho, L. M., Chan, W. S., Anderson, R. M., Hedley, A. J., and Leung, G. M. (2005). Methods for estimating the case fatality ratio for a novel, emerging infectious disease. *American Journal of Epidemiology*, 162(5):479–486.
- Gupte, P., Kucharski, A., Russell, T., Lambert, J., Gruson, H., Taylor, T., Azam, J., Degoot, A., and Funk, S. (2024). cfr: Estimate disease severity and case ascertainment. *Data Collection*. Comprehensive R Archive Network. <https://cran.r-project.org/package=cfr>.
- Horita, N. and Fukumoto, T. (2022). Global case fatality rate from COVID-19 has decreased by 96.8% during 2.5 years of the pandemic. *Journal of Medical Virology*, 95(1):e28231.
- Jahja, M., Chin, A., and Tibshirani, R. J. (2022). Real-time estimation of covid-19 infections: Deconvolution and sensor fusion. *Statistical Science*, 37(2):207–228.
- Jewell, N. P., Lei, X., Ghani, A. C., Donnelly, C. A., Leung, G. M., Ho, L.-M., Cowling, B. J., and Hedley, A. J. (2007). Non-parametric estimation of the case fatality ratio with competing risks data: An application to Severe Acute Respiratory Syndrome (SARS). *Statistics in Medicine*, 26(9):1982–1998.
- Kamp, J. and Krouse, S. (2020). Case-fatality metric points to increase in December deaths. *Wall Street Journal*.
- Lipsitch, M., Donnelly, C. A., Fraser, C., Blake, I. M., Cori, A., Dorigatti, I., Ferguson, N. M., Garske, T., Mills, H. L., Riley, S., Van Kerkhove, M. D., and Hernán, M. A. (2015). Potential biases in estimating absolute and relative case-fatality risks during outbreaks. *PLOS Neglected Tropical Diseases*, 9(7):e0003846.

- Liu, J., Cai, Z., Gustafson, P., and McDonald, D. J. (2024). Time-varying reproduction number estimation with trend filtering. *PLOS Computational Biology*.
- Liu, J., Wei, H., and He, D. (2023). Differences in case-fatality-rate of emerging SARS-CoV-2 variants. *Public Health in Practice*, 5:100350.
- Luo, G., Zhang, X., Zheng, H., and He, D. (2021). Infection fatality ratio and case fatality ratio of COVID-19. *International Journal of Infectious Diseases*, 113:43–46.
- Madrigal, A. C. and Moser, W. (2020). How many americans are about to die? *The Atlantic*.
- McNeil, D. G. J. (2020). The pandemic’s big mystery: How deadly is the coronavirus? *New York Times*.
- National Center for Health Statistics (NCHS) (2023). In-hospital mortality among hospital confirmed covid-19 encounters by week from selected hospitals. National Hospital Care Survey (NHCS).
- Nishiura, H., Klinkenberg, D., Roberts, M., and Heesterbeek, J. A. P. (2009). Early epidemiological assessment of the virulence of emerging infectious diseases: A case study of an Influenza pandemic. *PLOS One*, 4(8):e6852.
- Overton, C., Webb, L., Datta, U., Fursman, M., Hardstaff, J., Hiironen, I., Paranthaman, K., Riley, H., Sedgwick, J., Verne, J., Willner, S., Pellis, L., and Hall, I. (2022). Novel methods for estimating the instantaneous and overall COVID-19 case fatality risk among care home residents in England. *PLOS Computational Biology*, 18(10):e1010554.
- Qu, Y., Lee, C. Y., and Lam, K. F. (2022). A novel method to monitor covid-19 fatality rate in real-time, a key metric to guide public health policy. *Sci Rep*, 12:18277.
- Reich, N. G., Lessler, J., Cummings, D. A. T., and Brookmeyer, R. (2012). Estimating absolute and relative case fatality ratios from infectious disease surveillance data. *Biometrics*, 68(2):598–606. Published online 2012 Jan 25.
- Roth, G. A., Emmons-Bell, S., Alger, H. M., Bradley, S. M., Das, S. R., de Lemos, J. A., Gakidou, E., Elkind, M. S. V., Hay, S., Hall, J. L., Johnson, C. O., Morrow, D. A., Rodriguez, F., Rutan, C., Shakil, S., Sorensen, R., Stevens, L., Wang, T. Y., Walchok, J., Williams, J., and Murray, C. (2021). Trends in patient characteristics and COVID-19 in-hospital mortality in the United States during the COVID-19 pandemic. *JAMA Network Open*, 4(5):e218828.
- Russell, T. W., Hellewell, J., Abbott, S., Jarvis, C. I., van Zandvoort, K., Ratnayake, R., CMMID nCov working group, Flasche, S., Eggo, R., Edmunds, W. J., and Kucharski, A. J. (2020a). Using a Delay-Adjusted Case Fatality Ratio to Estimate Under-Reporting. *Fondazione Cerm*.
- Russell, T. W., Hellewell, J., Jarvis, C. I., van Zandvoort, K., Abbott, S., Ratnayake, R., CMMID COVID-19 working group, Flasche, S., Eggo, R. M., Edmunds, W. J., and Kucharski, A. J. (2020b). Estimating the infection and case fatality ratio for coronavirus disease (COVID-19) using age-adjusted data from the outbreak on the Diamond Princess cruise ship, February 2020. *Eurosurveillance*, 25(12):2000256.
- Thomas, B. S. and Marks, N. A. (2021). Estimating the case fatality ratio for covid-19 using a time-shifted distribution analysis. *Epidemiol Infect*, 149:e197.
- Tibshirani, R. J. (2014). Adaptive piecewise polynomial estimation via trend filtering. *The Annals of Statistics*, 42(1):285–323.
- Wallinga, J. and Lipsitch, M. (2007). How generation intervals shape the relationship between growth rates and reproductive numbers. *Proceedings of the Royal Society B: Biological Sciences*, 274(1609):599–604.
- Wallinga, J. and Teunis, P. (2004). Different epidemic curves for severe acute respiratory syndrome reveal similar impacts of control measures. *American Journal of Epidemiology*, 160(6):509–516.



- Ward, T. and Johnsen, A. (2021). Understanding an evolving pandemic: An analysis of the clinical time delay distributions of covid-19 in the united kingdom. *PLOS One*, 16(10):e0257978.
- Wjst, M. and Wendtner, C. (2023). High variability of COVID-19 case fatality rate in Germany. *BMC Public Health*, 23:416.
- Xie, Y., Choi, T., and Al-Aly, Z. (2024). Mortality in patients hospitalized for COVID-19 vs Influenza in fall-winter 2023-2024. *Journal of the American Medical Association*, 331(22):1963–1965.
- Yuan, J., Li, M., Lv, G., and Lud, Z. K. (2020). Monitoring transmissibility and mortality of COVID-19 in Europe. *Interational Journal of Infectious Diseases*, 95:311–315.
- Zhou, F., Yu, T., Du, R., Fan, G., Liu, Y., Liu, Z., Xiang, J., Wang, Y., Song, B., Gu, X., Guan, L., Wei, Y., Li, H., Wu, X., Xu, J., Tu, S., Zhang, Y., Chen, H., and Cao, B. (2020). Clinical course and risk factors for mortality of adult inpatients with covid-19 in wuhan, china: A retrospective cohort study. *The Lancet*, 395(10229):1054–1062.

## A Bias Proofs

We first prove Proposition 1, the bias of the oracle convolutional ratio.

*Proof.*

$$\begin{aligned}
\text{Bias}(\hat{p}_t^\pi) &= \mathbb{E}_t[\hat{p}_t^\pi] - p_t \\
&= \frac{\mathbb{E}_t[Y_t]}{\sum_{k=0}^d X_{t-k}\pi_k} - p_t \\
&= \frac{\sum_{k=0}^d X_{t-k}\pi_k p_{t-k}}{\sum_{k=0}^d X_{t-k}\pi_k} - \frac{p_t \sum_{k=0}^d X_{t-k}\pi_k}{\sum_{k=0}^d X_{t-k}\pi_k} \\
&= \sum_{k=0}^d \frac{X_{t-k}\pi_k}{\sum_{j=0}^d X_{t-j}\pi_j} (p_{t-k} - p_t).
\end{aligned}$$

□

The well-specified bias can be understood as a weighted average of  $\{p_{t-k} - p_t\}_{k=0}^d$ . The attainable absolute bias ranges between  $\min_{k=0,\dots,d} |p_{t-k} - p_t| = 0$ , achieved by  $k = 0$ , and  $\max_{k=0,\dots,d} |p_{t-k} - p_t|$ . This maximal bias is achieved by setting one of the weights  $X_{t-k}\pi_k / (\sum_{j=0}^d X_{t-j}\pi_j)$  to 1 and the rest to zero, either through the delay distribution  $\pi$  or through the primary incidence curve  $X$ . Hence, the explanations for delay distribution and primary incidence are aligned: They inflate the bias by upweighting distant timepoints for which the severity rate was different. If severity rates are monotonically changing, for example, then the maximal bias occurs at  $k = d$ .

Next, we prove the bias expression under misspecified delay distribution (Proposition 2).

*Proof.*

$$\begin{aligned}
\text{Bias}(\hat{p}_t^\gamma) &= \frac{\mathbb{E}_t[Y_t]}{\sum_{k=0}^d X_{t-k}\gamma_k} - p_t \\
&= \frac{\sum_{k=0}^d X_{t-k}\pi_k p_{t-k}}{\sum_{k=0}^d X_{t-k}\gamma_k} - \frac{\sum_{k=0}^d X_{t-k}\gamma_k p_t}{\sum_{k=0}^d X_{t-k}\gamma_k} \\
&= \sum_{k=0}^d \frac{X_{t-k}}{\sum_{j=0}^d X_{t-j}\gamma_j} (\pi_k p_{t-k} - \gamma_k p_t) \\
&= \sum_{k=0}^d \frac{X_{t-k}}{\sum_{j=0}^d X_{t-j}\gamma_j} (\pi_k p_{t-k} - (\pi_k + (\gamma_k - \pi_k)) p_t) \\
&= \frac{\sum_{j=0}^d X_{t-j}\pi_j}{\sum_{j=0}^d X_{t-j}\gamma_j} \sum_{k=0}^d \frac{X_{t-k}\pi_k}{\sum_{j=0}^d X_{t-j}\pi_j} (p_{t-k} - p_t) - \\
&\quad p_t \sum_{k=0}^d \frac{X_{t-k}}{\sum_{j=0}^d X_{t-j}\gamma_j} (\gamma_k - \pi_k) \\
&= \frac{\sum_{j=0}^d X_{t-j}\pi_j}{\sum_{j=0}^d X_{t-j}\gamma_j} \text{Bias}(\hat{p}_t^\pi) + p_t \left[ \frac{\sum_{k=0}^d X_{t-k}\pi_k}{\sum_{j=0}^d X_{t-j}\gamma_j} - 1 \right]
\end{aligned}$$

□

## B Alternative data sources

### B.1 Retrospective deaths

JHU presented daily deaths in real time, aligned by the date they were reported. In contrast, the National Center for Health Statistics (NCHS) provided weekly totals for deaths aligned by occurrence, and were not

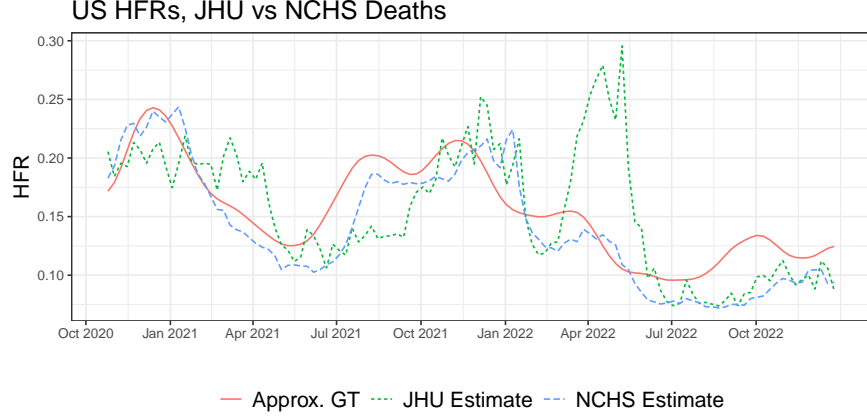


Figure 5: Real-time lagged ratios, JHU vs NCHS deaths. Seven-day smoothing with 19- and 11-day lags, respectively.

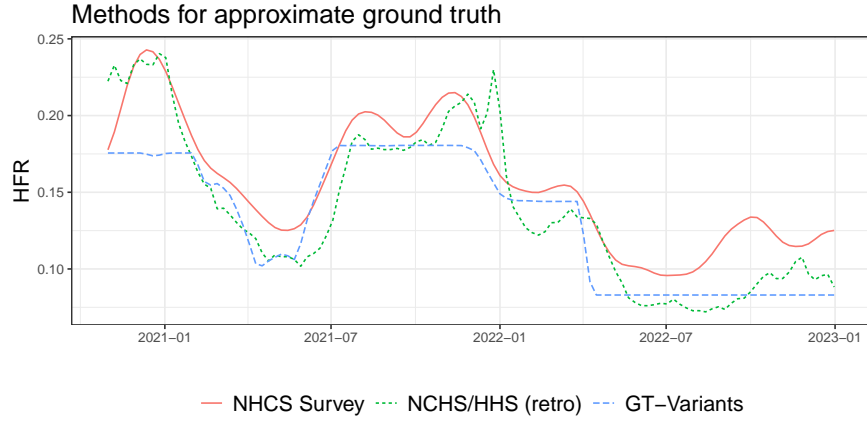


Figure 6: Methods for retrospective ground truth HFRs.

available in real time. Thus, delay distributions with NCHS deaths have a lighter tail.

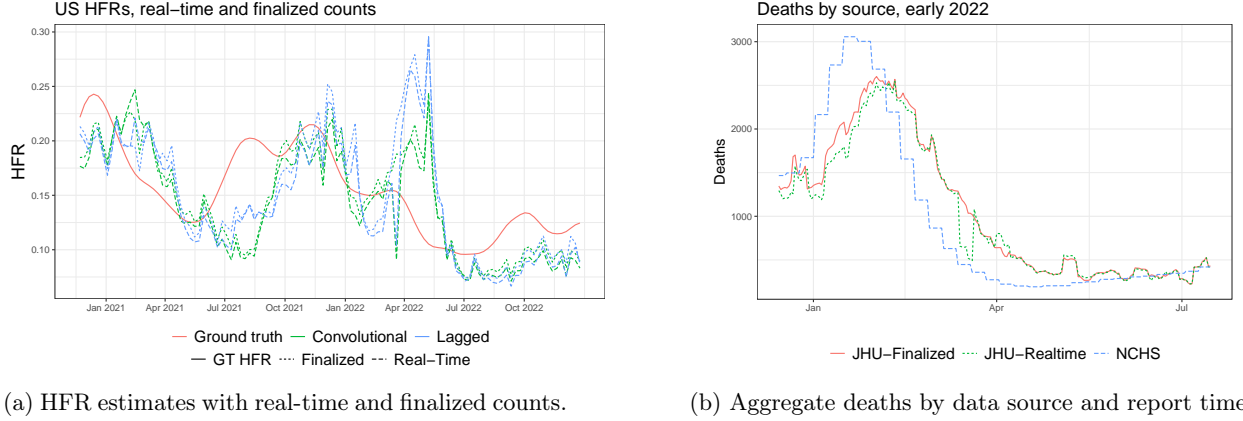
Figure 5 shows this minor change has a significant effect on the bias. It compares the real-time lagged ratios with deaths sourced from JHU and NCHS. JHU is much more biased during the variant periods discussed. For example, NCHS only rises from 12% to 14% as Omicron falls, far below JHU’s surge above 25%. As analyzed in Section 2.2, JHU’s heavier-tailed delay distribution inflates the influence of dates with higher HFRs than the present.

## B.2 Alternative ground truth

We considered two retrospective approaches to approximate the ground truth national HFRs over time. The first approach took lagged ratios with aggregate deaths from NCHS. NCHS is a better resource than JHU because it uses death counts from the date they actually occurred, not merely reported. In addition, we take a forward-looking ratio, which is retrospective insofar as it uses data after time  $t$  to estimate the HFR.

$$\hat{p}_t^{\text{LaggedRetro}} = \frac{Y_{t+L}}{X_t} \quad (8)$$

The second approach computed a single HFR for each major variant, then mixing by the proportions of variants in circulation. Formally, let  $\hat{p}_j$  approximate the HFR of variant  $j$ ; let  $v_t^j$  be its proportion of cases at time  $t$ , where  $\sum_j v_t^j = 1 \forall t$ . The HFR estimate is



(a) HFR estimates with real-time and finalized counts.

(b) Aggregate deaths by data source and report time.

Figure 7: Convolutional ratio estimates are biased regardless of which delay distribution is selected.

$$\hat{p}_t^{\text{Var}} = \sum_j v_t^j \hat{p}_j.$$

Each variant’s HFR  $\hat{p}_j$  was defined as the ratio of total NCHS deaths and HHS hospitalizations during the period where it accounted for over 50% of activate cases. The case proportions  $v_t^j$  were obtained from [covariants.org](#). To ensure estimates were reasonable, we only considered the 4 largest variants: The original strain, Alpha, Delta, and Omicron. Because Omicron began with an enormous surge that quickly subsided, we split it into early and late periods at April 1, 2022, following ([Adjei, Stacey and Hong, Kai and Molinari, Noelle-Angelique M and Bull-Otterson, Lara and Ajani, Umed A and Gundlapalli, Adi V and Harris, Aaron M and Hsu, Joy and Kadri, Sameer S and Starnes, Jon and Yeoman, Kristin and Boehmer, Tegan K, 2022](#)).

Figure 6 displays the three curves approximating the true HFRs. They have nontrivial differences in magnitude, but move more or less in conjunction. To validate our results, we primarily used the rescaled NCHS HFRs as the least problematic of the three. The retrospective NCHS ratios are subject to statistical bias, expressed in (7). The variant-based HFRs are flatter, as they do not account for other sources of variability. Therefore, they do not explain for the statistical bias within each variant period, which arises due to changes in the underlying severity rate.

## C Robustness checks

### C.1 Data source

The results in Section 3.1 use hospitalization and death counts available in real time. To investigate the sensitivity of our findings, we recomputed the lagged and convolutional ratios, this time using the finalized aggregates. Figure 7a shows the estimates with real-time and finalized counts track very closely to one another. Therefore, the observed bias in 3 cannot be attributed to reporting quirks.

The one period where the curves are significantly different from one another is in March 2022. While the HFRs from finalized counts steadily rise, the real-time estimates sharply fall then immediately bounce back. This sudden drop is due to a brief period in which reported death counts were suddenly too low (Fig. 7b). This is corrected in the finalized counts, hence their smooth HFRs. Removing this artifact further reinforces the bias trends described in Section 2.2.

### C.2 Hyperparameters

In this section we demonstrate the robustness of our findings against choices of hyperparameters. (All results are with the finalized version of JHU deaths.) First, Figure 8 plots performance over choices of window size parameter. We analyze smoothed versions of the lagged estimator

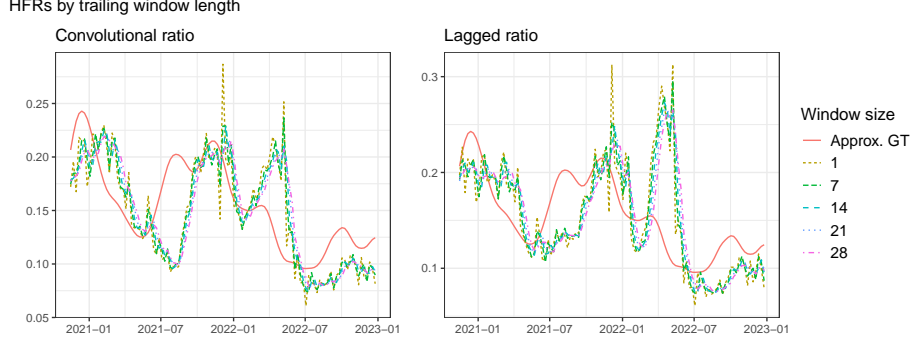


Figure 8: The length of the trailing window bears little impact on the findings.

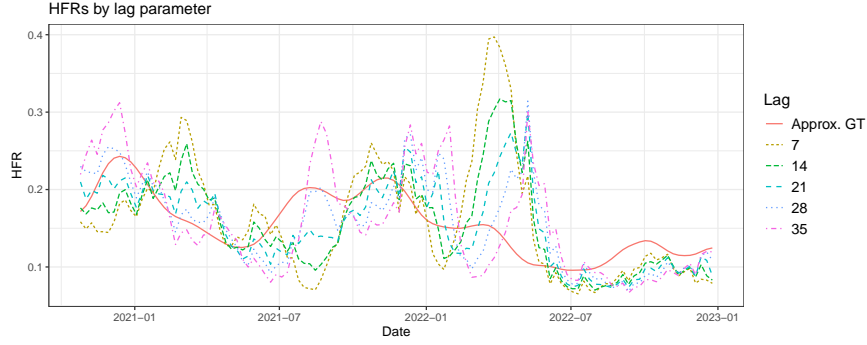


Figure 9: HFRs are biased regardless of what lag parameter is selected.

$$\hat{p}_t^{\ell, W} = \frac{\sum_{s=t-w+1}^t Y_s}{\sum_{s=t-w+1}^t X_{s-\ell}}, \quad (9)$$

as well as the convolutional estimator

$$\hat{\tilde{p}}_t^{\gamma, W} = \frac{\sum_{s=t-w+1}^t Y_s}{\sum_{s=t-w+1}^t \sum_{k=0}^d X_{s-\ell-k} \gamma_k}. \quad (10)$$

Results are very similar, indicating the bias does not disappear when smoothing over a longer history.

We next examine the time-to-death hyperparameters: The lag  $\ell$  for the lagged ratio and delay distribution  $\pi$  for the convolutional ratio. Figure 9 displays HFR estimates with lags ranging from 2 to 5 weeks. Unlike the window size, changing this parameter leads to different behavior across lags. Some choices are better than others; a 28-day lag, for example, falls appropriately in winter 2021 and rises less slowly during Delta. However, all are biased to varying degrees, most notably the huge spurious surge in spring 2022.

Figure 10 compares the performance of the convolutional ratio across different choices of delay distribution. We kept the discrete gamma shape for each, but varied the mean and standard deviation. As before, Figure 10a kept the standard deviation to 90% of the mean, per Ward and Johnsen (2021). We also evaluated with a more compact delay distribution in 10b.

All HFR estimates in the figures are significantly biased. Regardless of delay distribution, the ratios are negatively biased during the onset of Delta, and surge after the peak of Omicron. This indicates the bulk of the error is fundamental to the estimator, and cannot be attributed to model misspecification.

Comparing to the approximate ground truth HFRs from NHCS, performance improved slightly with a longer delay distribution than the purported mean of 20 days. Its mean absolute error was 0.031, whereas the delay distribution with mean 28 and standard deviation 25 had a MAE of 0.27. Nevertheless, this difference is relatively small, with the alternative delay distribution still showing similar bias.

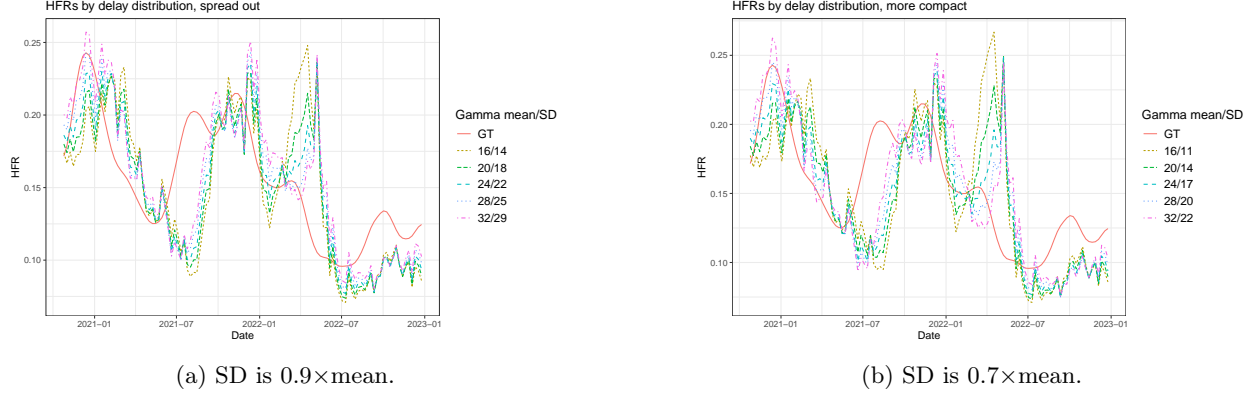


Figure 10: Convolutional ratio estimates are biased regardless of which delay distribution is selected.

### C.3 Geography

Next, we repeat our analysis on different geographies, finding similar trends. We repeated our computations on the 6 largest US states with the same lag and delay distribution, with finalized death counts from JHU. Because the NHCS survey was conducted on a subset of hospitals meant to represent the US at large, it may poorly approximate the HFRs for individual states. A better state-level source is the retrospective lagged ratio (8) using NCHS deaths. Figure 11 compares this rough ground truth with the real-time estimates. For both NCHS and JHU deaths, we again take the lag that maximizes cross-correlation with hospitalizations; the standard deviation of the delay distribution is 0.9 times the mean.

Several states have similar biases as the US results (Fig. 3a). Ratios in California, Texas, and Florida all are slow to detect the uptick in HFR during Delta; they also spike during Omicron in California, and to a lesser extent Florida. Note these states are the ones with the largest optimal lags, an estimate of the average time to death. As our simulated examples have shown, the shape of the delay distribution is a key factor behind the degree of bias. In contrast, New York, Pennsylvania, and Illinois have mean delays of at most 17. While their HFRs are still biased, they are relatively close to the NCHS curve. This suggests that fatality ratios are generally less trustworthy in states that take longer to report deaths.

## D Miscellaneous results

### D.1 Alternative lag on simulation

Figure 12 presents the simulation results from Section 3.2 when the lag is the mean of the delay distribution. It clearly indicates the lagged ratio is not markedly better under this lag. This is in step with Figure 9, which demonstrated that its performance on real data are robust to choice of lag.

### D.2 Further analysis

In this section, we present examples that further explain the well-specified bias. These are more contrived than the ones in Section 2.2, for example using unrealistic delay distributions. Nevertheless, their bias can be simplified to simple analytic formulas, isolating the three contributing factors.

To elucidate the relationship between changing severity rates and the ratio estimators' bias, consider the trivial case where all secondary events occur after exactly  $\ell$  days with no noise. By definition,  $\pi_k = \mathbf{1}\{k = \ell\}$ , so the convolutional and lagged ratios are both  $\hat{p}_t = \frac{X_{t-\ell} p_{t-\ell}}{X_{t-\ell}} = p_{t-\ell}$  presuming both have access to the oracle delay distribution. Figure 13a displays this with the approximate ground truth HFRs from NHCS.

In this case, the bias is the change in the true severity rate  $p_{t-\ell} - p_t$ . The estimator is unbiased only when the severity rate is stationary. Otherwise, for example, the ratio will be 20% too low if the true severity rate was 20% lower  $\ell$  days ago.

## State-level true & estimated HFRs

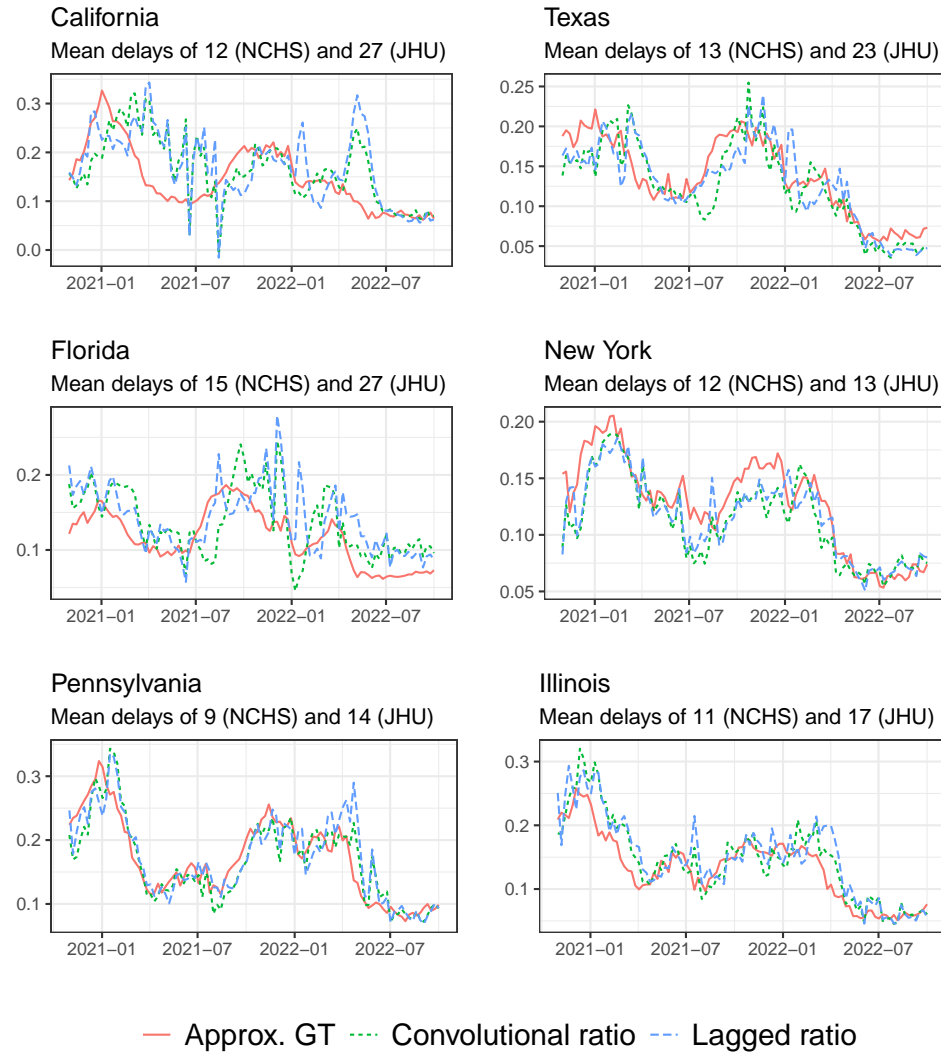


Figure 11: HFRs by individual states. Comparing retrospective estimates with NCHS against real-time estimates with JHU.



## HFRs, simulated deaths

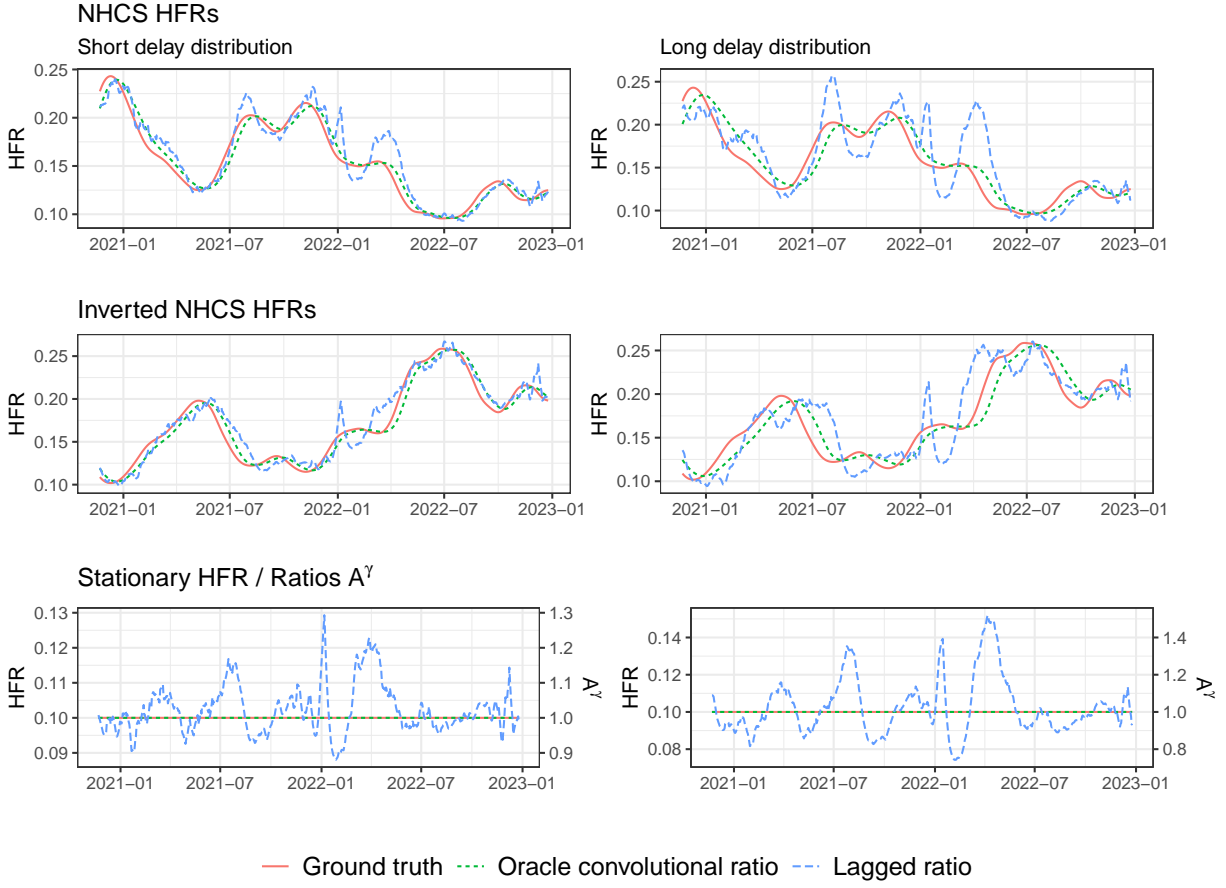
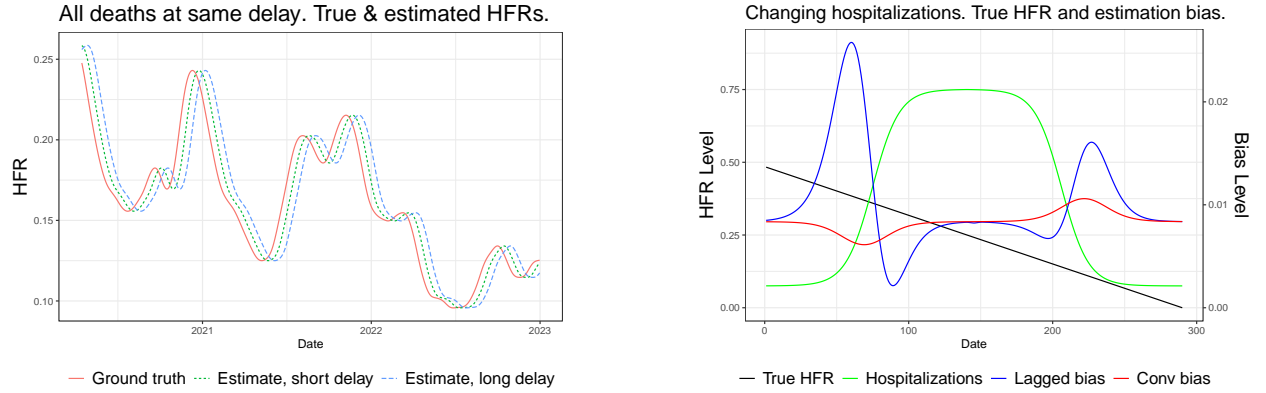


Figure 12: Lag chosen as mean of delay distribution. Same simulated data as Section 3.2.



(a) All deaths after  $\ell$  days. HFR ratios equivalent; plotting delays of  $\ell = 14$  and 28 days.

(b) Changing primary incidence. Plotting bias of lagged and convolutional ratios.

Figure 13: Toy examples of biased severity rates.

Intuitively, severity rates may be less similar to the present value  $p_t$  further back in time. In this simple example, the bias  $p_{t-\ell} - p_t$  is generally larger when  $\ell = 28$  than  $\ell = 14$  (Fig 13a). This expresses the observation that estimates with heavier-tailed delay distributions tend to have more bias.

Section 2.2 claims that changes in primary incidence levels affect the magnitude of bias for the convolutional ratio. Here, we present simple examples that formalize this claim. First assume primary incidence is constant, in which case the convolutional and lagged ratios are equal. The time series factors neatly out of the bias expression Proposition 1:

$$\text{Bias}(\hat{p}_t^\gamma) = \text{Bias}(\hat{p}_t^\ell) = \left( \sum_{k=0}^d \pi_k p_{t-k} \right) - p_t.$$

This is the difference between a weighted average of previous severity rates and the present. Weights for the historical rates are given by the delay distribution, providing further justification for its central role in the bias.

Next, suppose half of the secondary events occur immediately after the primary event ( $t = 0$ ), and the other half after  $d$  days. Further assume  $p_{t-d} \neq p_t$ , so there is some degree of bias. Then

$$\begin{aligned} |\text{Bias}(\hat{p}_t^\gamma)| &= \frac{\frac{1}{2}|X_t(p_t - p_t) + X_{t-d}(p_{t-d} - p_t)|}{\frac{1}{2}(X_t + X_{t-d})} \\ &= \frac{X_{t-d}|p_{t-d} - p_t|}{X_{t-d}(1 + \frac{X_t}{X_{t-d}})} = \frac{|p_{t-d} - p_t|}{1 + \frac{X_t}{X_{t-d}}} \end{aligned}$$

The absolute bias is monotonically decreasing in  $\frac{X_t}{X_{t-d}}$ , the proportion change in primary incidence. Rising primary incidence ( $\frac{X_t}{X_{t-d}} > 1$ ) yields less bias, while falling levels yield more.

Figure 13b displays this setting. Hospitalizations are defined as  $X = \sigma(s) * 9000 + 1000$ , where  $\sigma$  is the sigmoid function and  $s$  takes 300 evenly spaced steps from -9 to 7. The true HFRs fall from 0.5 to 0 over the same number of even steps. Indeed, the convolutional ratio's bias dips as hospitalizations rise, and rises as they fall.

The figure also plots with lagged ratio with  $\ell = \frac{d}{2}$ , the mean of the delay distribution. When daily hospitalizations are close to constant, the two estimators converge towards the same ratio. During periods of change, however, the lagged estimator has different bias. It first moves upwards — the opposite direction as the convolutional bias — with far greater magnitude. This can be explained by the ratio  $A_t^\ell = \frac{X_{t-2\ell} + X_t}{2X_{t-\ell}}$  from Proposition 2. As hospitalizations begin to steeply rise,  $X_{t-2\ell}$  and  $X_{t-\ell}$  are similar, but  $X_t > X_{t-\ell}$ . Hence,  $A_t^\ell > 1$ , contributing positive bias to both the oracle and misspecification terms. As hospitalizations level out near the top,  $A_t^\ell < 1$ , hence the bias falling lower. The opposite pattern occurs as hospitalizations fall.